

Supervised Functional PCA with Covariate Dependent Mean and Covariance Structure

Fei Ding

Institute of Statistics and Big Data, Renmin University of China

Department of Statistics, Texas A&M University

Shiyuan He

Institute of Statistics and Big Data, Renmin University of China

David E. Jones

Department of Statistics, Texas A&M University

and

Jianhua Z. Huang

Department of Statistics, Texas A&M University

January 31, 2020

Abstract

Incorporating covariate information into functional data analysis methods can substantially improve modeling and prediction performance. However, many functional data analysis methods do not make use of covariate or *supervision* information, and those that do often have high computational cost or assume that only the scores are related to covariates, an assumption that is usually violated in practice. In this article, we propose a functional data analysis framework that relates both the mean and covariance function to covariate information. To facilitate modeling and ensure the covariance function is positive semi-definite, we represent it using splines and design a map from Euclidean space to the symmetric positive semi-definite matrix manifold. Our model is combined with a roughness penalty to encourage smoothness of the estimated functions in both the temporal and covariate domains. We also develop an efficient method for fast evaluation of the objective and gradient functions. Cross-validation is used to choose the tuning parameters. We demonstrate the advantages of our approach through a simulation study and an astronomical data analysis.

Keywords: Astrostatistics; Computational efficiency; Covariate information; Penalized likelihood; Supervised functional principal component analysis

1 Introduction

Functional data analysis (FDA) is becoming increasingly important in many scientific fields, including astronomy, biology, and neuroscience. FDA is a powerful tool for sparse and irregularly sampled time series data, spatial data and some high dimensional data. It treats observations as functions, or elements in a Hilbert space, and exploits the underlying smoothness to model the data efficiently. Due to the prevalence of different types of functional data and the associated computational challenges, many functional data analysis (FDA) methods have been developed, see Ramsay and Silverman (2005) for an overview.

Among the FDA methods, functional principal component analysis (FPCA) plays a pivotal role because from a modeling, scientific, or computational perspective it is often necessary to reduce the dimensionality of the data. Indeed, FPCA has been an important tool for many years and there are well-established modeling frameworks and fitting algorithms for its different variants. A popular FPCA approach is based on the work of James et al. (2000), which established a mixed effects modeling framework for irregular and sparse functional data. Estimating several leading functional principle components (FPCs) is equivalent to estimating a covariance function with low rank structure, and Peng and Paul (2009) proposed estimating FPCs with a restricted maximum likelihood (REML) method. Paul et al. (2009) established consistency and the rate of convergence for the REML estimator. Cai and Yuan (2010) proposed to estimate the covariance function in reproducing kernel Hilbert space. The work of Yao et al. (2005) is another classical approach that estimates the covariance function via a local smoothing technique. In the Bayesian framework, Suarez et al. (2017) proposed an alternative PCA based method that approximates the covariance matrix eigenfunctions using spectral decomposition. Van Der Linde (2008) suggested a Bayesian approach to FDA, overcoming the associated computational challenges by use of variational inference.

Due to the fundamental importance of FPCA, these methods have been extended in various directions. Among them multi-dimensional FPCA has particularly attracted interest. Some studies have characterized the relationship between multiple or paired longitudinal curves, e.g., Zhou et al. (2008) provided a framework to jointly model paired longitudinally observed variables using PCA scores. Kayano and Konishi (2009) explored multi-dimensional functional data estimation strategies based on Gaussian basis functions. Di et al. (2009) considered multi-level FPCA for intra- and inter-subject variations.

Supervised functional data methods have also gained popularity. Functional observations are often coupled with additional covariate information. By incorporating additional covariate information, FDA models and their prediction accuracy can be substantially improved. The majority of these approaches are based on Yao et al. (2005). For example, Jiang et al. (2010) proposed an approach to accommodate covariate information using a local linear smoother. Other related work includes Jiang et al. (2011), Zhang et al. (2013), and Zhang et al. (2016). However, these methods all have limitations because the local smoothing approach is usually accompanied with high computational cost and is not scalable to big data contexts.

In this paper we develop a supervised FPCA framework to incorporate covariate information in a computationally efficient manner. We call our method *supervised functional*

PCA with a symmetric positive semi-definite manifold structure, or SFPDM for short. Our method is an extension of the supervised sparse and functional principal component (SupSFPC) method proposed by Li et al. (2016). SupSFPC incorporates supervision information by assuming that the principle component (PC) scores vary linearly with covariates. However, the linear restriction and only allowing dependence on the covariates through the scores creates limitations and both assumptions are often violated in practice. Also, SupSFPC cannot handle irregularly spaced functional data. Our method does not have these limitations and outperforms SupSFPC in all our numerical studies. In particular, in our method both the mean function and covariance function are allowed to depend on the covariates in a non-linear way. In the case of the covariance function, non-linearity is achieved by allowing the underlying principal components (eigenfunctions) as well as the eigenvalues to depend on the covariates. This development leads to the technical challenge of ensuring the implied covariance function is positive semi-definite. After representing the covariance function with splines, the requirement is equivalent to ensuring the related covariance matrix is symmetric positive semi-definite. We overcome the challenge by designing a map from Euclidean space to the symmetric positive semi-definite matrix manifold.

We now briefly review the classical FPCA framework to further explain our contributions. We denote by $x_n(t)$ the value of an underlying latent function at time t , for $n = 1, \dots, N$. More generally, we could consider functions of other types of variable, such as location, but here restrict our attention to functions of time. For each function $x_n(t)$, its covariance function $\text{cov}(x_n(t), x_n(t')) = G(t, t')$ has eigenvalue-eigenfunction decomposition $G(t, t') = \sum_{k=1}^{\infty} d_k f_k(t) f_k(t')$, where f_k is the corresponding k -th eigenfunction and d_k is the k -th eigenvalue. The eigenfunctions are orthonormal to each other, and the eigenvalues are ordered nonincreasingly $d_1 \geq d_2 \geq d_3 \geq \dots$. By the *Karhunen – Loève* theorem, the function $x_n(t)$ can be expressed by a linear combination of a mean function and eigenfunctions, i.e., $x_n(t) = \mu(t) + \sum_{j=1}^{\infty} \xi_j^{(n)} f_j(t)$, where $\xi_j^{(n)} = \int x_n(t) f_j(t) dt$ is a random variable with mean 0 and variance d_j . Following James et al. (2000) we consider a mixed effects model for functional data in which the latent curves are approximated by a mean function and a small number of principal components, i.e.,

$$y_n(t) = x_n(t) + \epsilon(t) \approx \mu(t) + \sum_{j=1}^r \xi_j^{(n)} f_j(t) + \epsilon(t) = \mu(t) + \mathbf{f}^T(t) \boldsymbol{\xi}^{(n)} + \epsilon(t), \quad (1)$$

where $\mu(t)$ is the mean function, $f_j(t)$ is the j -th eigenfunction of the covariance function with eigenvalue d_j , and $\xi_j^{(n)}$ is the j -th score with $\xi_j \sim \mathbb{N}(0, d_j)$, for $j = 1, \dots, r$. Lastly, $\epsilon(t)$ denotes white noise with mean 0 and variance σ_{ϵ}^2 . On the right side of (1), we have used the vector notation $\mathbf{f}(t) = (f_1(t), \dots, f_r(t))^T$ and $\boldsymbol{\xi}^{(n)} = (\xi_1^{(n)}, \dots, \xi_r^{(n)})^T$. As data collection explodes in many areas, more and more functional data are accompanied by covariates \mathbf{z} . However, the mean function and eigenfunctions used by the above classical FPCA method do not depend on covariates. In our approach both the mean function and the covariance structure depend on the covariates, which is achieved using spline bases. In the spline basis representation, the positive semi-definite property of the covariance function corresponds to the symmetric positive semi-definiteness of a matrix $\boldsymbol{\Sigma}$ (see Section 2.2), and we ensure the latter by constructing a map from Euclidean space to the symmetric positive semi-definite

matrix manifold. Some recent papers have explored methods to model manifold-valued data, e.g., Lin et al. (2017). Roughness penalties also play a substantial role in our method to allow continuous control over smoothness. In contrast to this penalty approach, controlling smoothness by limiting the number of basis functions is discontinuous in nature, and is therefore less satisfactory. The penalty employed here encourages the estimated functions to be smooth in both the temporal and covariate domains.

This article is organized as follows. Section 2 presents our model for the mean and covariance functions, and introduces a penalty similar to that proposed by Wood (2006). Section 3 details our algorithm, which makes use of several approximations to reduce computational cost. In Sections 4 and 5, we compare our method with SupSFPC through a simulation study and an astronomical data analysis. Brief discussion is found in Section 6.

2 Supervised FPCA Model

Suppose that there are N latent functions of interest, denoted by x_n , for $n = 1, \dots, N$. For each latent function x_n , suppose that we have noisy observations at the sparse time points $t_1^{(n)}, \dots, t_{m_n}^{(n)}$, denoted by $\mathbf{y}_n = (y_n(t_1^{(n)}), \dots, y_n(t_{m_n}^{(n)}))^T$. All the time points are assumed to reside in a compact domain $\mathcal{T} = [t_{\min}, t_{\max}]$. Lastly, suppose that covariates $\mathbf{z}_n \in \mathcal{Z}$ are recorded along with \mathbf{y}_n , for each $n = 1, \dots, N$, where \mathcal{Z} is also a compact domain.

We construct a supervised FPCA model for such data. Instead of (1), we consider the following low rank model

$$y_n(t, \mathbf{z}) \approx \mu(t, \mathbf{z}) + \sum_{j=1}^r f_j(t, \mathbf{z}) \xi_j^{(n)} + \epsilon(t). \quad (2)$$

Both the mean function $\mu(t, \mathbf{z})$ and principal component functions $f_j(t, \mathbf{z})$ are allowed to vary smoothly with the covariates \mathbf{z} . The score vector $\boldsymbol{\xi}^{(n)} = (\xi_1^{(n)}, \dots, \xi_r^{(n)})^T \sim \mathbb{N}(\mathbf{0}, \mathbf{D}_\mathbf{z})$ follows a Gaussian distribution with mean zero and covariance matrix $\mathbf{D}_\mathbf{z}$ which also depends on \mathbf{z} . This implies that the covariance function of the latent process is $G(t, t' | \mathbf{z}) = \mathbf{f}^T(t, \mathbf{z}) \mathbf{D}_\mathbf{z} \mathbf{f}(t', \mathbf{z})$, with $f_j(t, \mathbf{z})$, for $j = 1, \dots, r$, being the elements of the vector $\mathbf{f}(t', \mathbf{z})$. For each \mathbf{z} , the rank of the covariance function $G(t, t' | \mathbf{z})$ is r . This low-rank structure is reasonable because in most cases a small number of eigenfunctions (e.g., two or three) capture most of the data variation.

2.1 Supervised Mean Function

Our model allows the mean function $\mu(t, \mathbf{z})$ in (2) to vary smoothly with both time t and the covariates \mathbf{z} . This is achieved using a tensor product spline basis, as we now explain. Firstly, dependence on t is captured by a cubic spline with l' equally spaced knots in the temporal domain \mathcal{T} , i.e., with $l = l' + 4$ degrees of freedom. Similarly, dependence on the covariates \mathbf{z} is captured using a cubic spline with p' knots, and therefore $p = p' + 4$ degrees of freedom. In our implementation, these splines are represented using B-spline bases, because computational methods for B-Splines and derivatives thereof are well developed, see Butterfield (1976) and De Boor (1977). Let $\mathbf{a}(t) \in \mathbb{R}^l$ and $\mathbf{u}(\mathbf{z}) \in \mathbb{R}^p$ be the values of

the B-spline basis functions evaluated at t and \mathbf{z} , respectively, e.g., the i -th entry of $\mathbf{a}(t)$ is the value of the i -th temporal domain B-spline basis function evaluated at t . With this notation, our proposed mean function is given by

$$\mu(t, \mathbf{z}) = \mathbf{a}(t)^T \boldsymbol{\Theta}_\mu \mathbf{u}(\mathbf{z}) = \sum_{i=1}^l \sum_{j=1}^p a_i(t) u_j(\mathbf{z}) \theta_{ij} = \mathbf{H}(t, \mathbf{z})^T \boldsymbol{\theta}_\mu, \quad (3)$$

where $\boldsymbol{\Theta}_\mu = (\theta_{ij}) \in \mathbb{R}^{l \times p}$ is the matrix of B-spline basis coefficients, $\mathbf{H}(t, \mathbf{z}) = \mathbf{a}(t) \otimes \mathbf{u}(\mathbf{z})$ is a tensor product spline basis, and $\boldsymbol{\theta}_\mu = \text{vec}(\boldsymbol{\Theta}_\mu)$, i.e., the vectorization of the coefficients matrix $\boldsymbol{\Theta}_\mu$.

2.2 Supervised Covariance Function

To model the covariance $G(t, t' | \mathbf{z})$, we rely on an orthonormalized B-spline basis, whose function values at t are denoted $\mathbf{b}(t) \in \mathbb{R}^m$, and which has the property that $\int_{\mathcal{T}} \mathbf{b}(t) \mathbf{b}(t)^T dt = \mathbf{I}$, where \mathbf{I} denotes the identity matrix. The orthonormalization of the B-spline basis enables us to easily obtain the eigenfunctions after training our model. With this basis, our covariance function is constructed as

$$G(t, t' | \mathbf{z}) = \mathbf{b}(t)^T \boldsymbol{\Sigma}(\mathbf{z}; \boldsymbol{\beta}) \mathbf{b}(t), \quad (4)$$

where $\boldsymbol{\Sigma}(\mathbf{z}; \boldsymbol{\beta}) \in \mathbb{R}^{m \times m}$ is a matrix that depends on the covariates \mathbf{z} and parameterized by coefficients $\boldsymbol{\beta}$.

We must ensure that our covariance function G in (4) is positive semi-definite. This is equivalent to requiring $\boldsymbol{\Sigma}(\mathbf{z}; \boldsymbol{\beta})$ to be a positive semi-definite matrix for each \mathbf{z} . Using ideas in Zhu et al. (2009), we construct $\boldsymbol{\Sigma}(\cdot; \boldsymbol{\beta})$ using a map from \mathcal{Z} to the symmetric positive semi-definite matrix manifold $\text{Sym}^+(m)$, i.e.

$$\boldsymbol{\Sigma}(\cdot; \boldsymbol{\beta}) : \mathbf{z} \mapsto \boldsymbol{\Sigma}(\mathbf{z}; \boldsymbol{\beta}) = \mathbf{C}(\mathbf{z}; \boldsymbol{\beta}) \mathbf{C}(\mathbf{z}; \boldsymbol{\beta})^T. \quad (5)$$

In the above, $\mathbf{C}(\mathbf{z}; \boldsymbol{\beta}) \in \mathbb{R}^{m \times r}$ depends on the covariates \mathbf{z} and the unknown coefficient $\boldsymbol{\beta}$. The structure (5) is similar to that of Cholesky decomposition, except that the matrix $\mathbf{C}(\mathbf{z}; \boldsymbol{\beta})$ is not required to be lower triangular. In fact, by setting $r < m$, the rank of $\boldsymbol{\Sigma}(\mathbf{z}; \boldsymbol{\beta})$ is at most r at each \mathbf{z} .

With the help of (5), the construction of a positive semi-definite $\boldsymbol{\Sigma}(\mathbf{z}; \boldsymbol{\beta})$ is reduced to the construction of a general matrix $\mathbf{C}(\mathbf{z}; \boldsymbol{\beta})$ without restriction. Notice that each entry c_{ij} of \mathbf{C} is a function of \mathbf{z} . Specifically, for $i = 1, \dots, m$ and $j = 1, \dots, r$, we model $c_{ij} = \mathbf{v}(\mathbf{z})^T \boldsymbol{\beta}_{ij}$ with a B-spline basis $\mathbf{v}(\cdot) \in \mathbb{R}^q$ and the corresponding coefficients $\boldsymbol{\beta}_{ij} \in \mathbb{R}^q$. In summary, our model construction of $\mathbf{C}(\mathbf{z}; \boldsymbol{\beta})$ (and hence $\boldsymbol{\Sigma}(\mathbf{z}; \boldsymbol{\beta})$) has $q \times m \times r$ unknown parameters, which are collected in a matrix $\boldsymbol{\Gamma} \in \mathbb{R}^{(mq) \times r}$:

$$\boldsymbol{\Gamma} = \begin{pmatrix} \boldsymbol{\beta}_{11} & \boldsymbol{\beta}_{12} & \cdots & \boldsymbol{\beta}_{1r} \\ \boldsymbol{\beta}_{21} & \boldsymbol{\beta}_{22} & \cdots & \boldsymbol{\beta}_{2r} \\ \vdots & \vdots & \ddots & \vdots \\ \boldsymbol{\beta}_{m1} & \boldsymbol{\beta}_{m2} & \cdots & \boldsymbol{\beta}_{mr} \end{pmatrix}. \quad (6)$$

Let $\boldsymbol{\beta} = \text{vec}(\boldsymbol{\Gamma})$ denote the vectorized version of this matrix. It readily follows that the factor matrix $\mathbf{C}(\mathbf{z}; \boldsymbol{\beta})$ in (5) can be written as $\mathbf{C}(\mathbf{z}; \boldsymbol{\beta}) = (\mathbf{I}_m \otimes \mathbf{v}(\mathbf{z})^T) \boldsymbol{\Gamma}$.

2.3 Model Likelihood

With the construction of the mean function and covariance function, we are able to write our complete model as

$$y_n(t, \mathbf{z}) = \underbrace{\mathbf{H}(t, \mathbf{z})^T \boldsymbol{\theta}_\mu + \mathbf{b}(t)^T \mathbf{C}(\mathbf{z}; \boldsymbol{\beta}) \boldsymbol{\psi}^{(n)}}_{x_n(t, \mathbf{z})} + \epsilon(t), \quad (7)$$

where $\boldsymbol{\psi}^{(n)} \sim \mathcal{N}(\mathbf{0}, \mathbf{I})$ is r -dimensional random vector and $\epsilon(t) \sim \mathcal{N}(0, \sigma_e^2)$ is white noise. From the above, the covariance function of the latent $x_n(t, \mathbf{z})$ is exactly $G(t, t' | \mathbf{z}) = \mathbf{b}(t)^T \mathbf{C}(\mathbf{z}; \boldsymbol{\beta}) \mathbf{C}(\mathbf{z}; \boldsymbol{\beta})^T \mathbf{b}(t')$. It is easy to verify that $y_n(t, \mathbf{z})$ follows a Gaussian distribution with mean $\mathbf{H}(t, \mathbf{z}) \boldsymbol{\theta}_\mu$ and variance $\mathbf{b}(t)^T \boldsymbol{\Sigma}(\mathbf{z}; \boldsymbol{\beta}) \mathbf{b}(t) + \sigma_e^2$.

When considering multiple observation times t_1, \dots, t_{m_n} for the n -th observation, we simplify notation by collecting the basis evaluations $\mathbf{b}(t_i^{(n)})$ for the covariance function (see (4)) and the tensor product basis evaluations $\mathbf{H}(t_i^{(n)}, \mathbf{z}_n)$ for the mean function (see (3)) into matrices \mathbf{B}_n and \mathbf{H}_n , respectively, i.e.,

$$\mathbf{B}_n = (\mathbf{b}(t_1^{(n)}), \mathbf{b}(t_2^{(n)}), \dots, \mathbf{b}(t_{m_n}^{(n)}))^T, \quad (8)$$

and

$$\mathbf{H}_n = (\mathbf{H}(t_1^{(n)}, \mathbf{z}_n), \mathbf{H}(t_2^{(n)}, \mathbf{z}_n), \dots, \mathbf{H}(t_{m_n}^{(n)}, \mathbf{z}_n))^T. \quad (9)$$

Now, for the n -th observation, the observed value vector $\mathbf{y}_n = (y_n(t_1^{(n)}), \dots, y_n(t_{m_n}^{(n)}))^T$ follows a multivariate Gaussian with mean $\mathbf{H}_n \boldsymbol{\theta}_\mu$ and covariance matrix $\boldsymbol{\Sigma}_n = \mathbf{B}_n \mathbf{C}_n \mathbf{C}_n^T \mathbf{B}_n^T + \sigma_e^2 \mathbf{I}$ with $\mathbf{C}_n = \mathbf{C}(\mathbf{z}_n, \boldsymbol{\beta})$. As a result, all unknown parameters can be estimated by minimizing the negative log-likelihood of all the observations

$$\mathcal{L}(\boldsymbol{\theta}_\mu, \boldsymbol{\beta}) = \sum_{n=1}^N -\log L(\mathbf{y}_n, \mathbf{z}_n) = \sum_{n=1}^N \{\log \det \boldsymbol{\Sigma}_n + \text{tr}(\mathbf{S}_n \boldsymbol{\Sigma}_n^{-1})\}, \quad (10)$$

with $\mathbf{S}_n = (\mathbf{y}_n - \mathbf{H}_n \boldsymbol{\theta}_\mu)(\mathbf{y}_n - \mathbf{H}_n \boldsymbol{\theta}_\mu)^T$.

Suppose $\hat{\boldsymbol{\theta}}_\mu$ and $\hat{\boldsymbol{\beta}}$ are the resulting maximum likelihood estimator of the parameters. Each estimated principal component function $\hat{f}_j(t, \mathbf{z})$ is computed as follows. At fixed \mathbf{z} , compute the matrix $\boldsymbol{\Sigma}(\mathbf{z}; \hat{\boldsymbol{\beta}}) = \mathbf{C}(\mathbf{z}; \hat{\boldsymbol{\beta}}) \mathbf{C}(\mathbf{z}; \hat{\boldsymbol{\beta}})^T$ with the estimator $\hat{\boldsymbol{\beta}}$ plugged-in, and evaluate the eigendecomposition of $\boldsymbol{\Sigma}(\mathbf{z}; \hat{\boldsymbol{\beta}})$. Suppose $\hat{\mathbf{v}}_j$ is the eigenvector corresponding to the j -th largest eigenvalue, then we get the estimated j -th eigenfunction as $\hat{f}_j(t, \mathbf{z}) = \mathbf{b}(t)^T \hat{\mathbf{v}}_j$. Note the eigenvector $\hat{\mathbf{v}}_j$ implicitly depends on the covariates \mathbf{z} through the decomposition of $\boldsymbol{\Sigma}(\mathbf{z}; \hat{\boldsymbol{\beta}})$. In addition, at fixed \mathbf{z} , the estimated eigenfunctions are orthonormal to each other, because the eigenvectors ($\hat{\mathbf{v}}_j$'s) are orthonormal to each other and $\mathbf{b}(\cdot)$ is an orthonormal basis.

2.4 Roughness Penalty

To encourage smoothness of the estimated mean function and covariance function, we add an additional roughness penalty to the negative log-likelihood (10). The classical

roughness penalty for an arbitrary function g is $J_t(g) = \int_a^b g''(t)^2 dt$. This penalty encourages the integrated second order derivative of g to be small. If g has a basis representation $g(t) = \sum_{k=1}^K \tilde{\alpha}_k \phi_k(t) = \tilde{\alpha}^T \phi(t)$ for some basis $\phi(\cdot)$ and related coefficient $\tilde{\alpha}$, then the penalty $J_t(g)$ can be directly evaluated by

$$J_t(g) = \tilde{\alpha}^T \int_a^b \left[\frac{\partial^2}{\partial t^2} \phi(t) \right] \left[\frac{\partial^2}{\partial t^2} \phi^T(t) \right] dt \tilde{\alpha} = \tilde{\alpha}^T \mathbf{S}_t \tilde{\alpha}. \quad (11)$$

In the above, $\mathbf{S}_t = \int_a^b \left[\frac{\partial^2}{\partial t^2} \phi(t) \right] \left[\frac{\partial^2}{\partial t^2} \phi^T(t) \right] dt$ is a fixed matrix with the given basis $\phi(t)$.

This classical penalty is not directly applicable to our setting, because our mean function and eigenfunctions depend on the unknown covariate \mathbf{z} , in addition to time t . We follow Wood (2006) to develop a computationally efficient penalty for multivariate functions. From the representation (7), $\mathbf{C}^T(\mathbf{z}; \boldsymbol{\beta}) \mathbf{b}(t)$ is a r dimensional collection of functions. We denote its j -th function as $h_j(t, \mathbf{z})$ for $j = 1, \dots, r$. As a result, the covariance function is $G(t, t' | \mathbf{z}) = \mathbf{b}(t)^T \mathbf{C}(\mathbf{z}; \boldsymbol{\beta}) \mathbf{C}^T(\mathbf{z}; \boldsymbol{\beta}) \mathbf{b}(t') = \sum_{j=1}^r h_j(t, \mathbf{z}) h_j(t', \mathbf{z})$. The smoothness of the estimated covariance function is achieved by penalizing on $h_j(t, \mathbf{z})$'s. Following Wood (2006), our penalty is computed by

$$J(h) = \lambda_t \sum_{j=1}^r \int_{\mathbf{z}} J_t(h_{t|\mathbf{z}}^{(j)}) d\mathbf{z} + \lambda_{\mathbf{z}} \sum_{j=1}^r \int_t J_{\mathbf{z}}(h_{\mathbf{z}|t}^{(j)}) dt, \quad (12)$$

with tuning parameters λ_t and $\lambda_{\mathbf{z}}$ to be determined by cross-validation. In the above, for a fixed \mathbf{z} , $h_{t|\mathbf{z}}^{(j)}(t) = h_j(t, \mathbf{z})$ is viewed as a function of time t . The penalty $J_t(h_{t|\mathbf{z}}^{(j)})$ evaluates the roughness of $h_{t|\mathbf{z}}^{(j)}$ by plugging this function into (11). Similarly, the penalty $J_{\mathbf{z}}(h_{\mathbf{z}|t}^{(j)})$ treats $h_{\mathbf{z}|t}^{(j)}(\mathbf{z}) = h_j(t, \mathbf{z})$ as a function of \mathbf{z} for fixed t . It evaluates the integrated squared value of the second order derivative of $h_{\mathbf{z}|t}^{(j)}$ with respect to \mathbf{z} .

In the interest of computational tractability, we write the functions $h_{t|\mathbf{z}}^{(j)}(t)$ in terms of the temporal and covariate domain B-spline bases introduced in Section 2.2, i.e.,

$$h_{t|\mathbf{z}}^{(j)}(t) = \sum_{i=1}^m \tilde{\alpha}_i^{(j)}(\mathbf{z}) b_i(t) = \tilde{\alpha}^{(j)}(\mathbf{z})^T \mathbf{b}(t), \quad (13)$$

where $\tilde{\alpha}_i^{(j)}(\mathbf{z}) = \sum_{l=1}^q (\boldsymbol{\beta}_{ij})_{il} v_l(\mathbf{z}) = \boldsymbol{\beta}_{ij}^T \mathbf{v}(\mathbf{z})$, and $\boldsymbol{\beta}_{ij}$ is the $q \times 1$ sub-matrix of $\boldsymbol{\Gamma}$ indicated in (6), for $j = 1, \dots, r$ and $i = 1, \dots, m$. Notice (13) can be viewed as varying coefficient representation of the function $h_{t|\mathbf{z}}^{(j)}(t)$. It follows that $\tilde{\alpha}^{(j)}(\mathbf{z}) = \mathbf{M}_{\mathbf{z}} \boldsymbol{\beta}^{(j)}$ where $\mathbf{M}_{\mathbf{z}} = \mathbf{I}_m \otimes \mathbf{v}^T(\mathbf{z})$ and $\boldsymbol{\beta}^{(j)}$ is the j -th column of coefficients matrix $\boldsymbol{\Gamma}$ in (6). According to (11), the penalty $J_t(h_{t|\mathbf{z}}^{(j)})$ can then be expressed as

$$J_t(h_{t|\mathbf{z}}^{(j)}) = \tilde{\alpha}^{(j)}(\mathbf{z})^T \mathbf{S}_t \tilde{\alpha}^{(j)}(\mathbf{z}) = \boldsymbol{\beta}^{(j)T} \mathbf{M}_{\mathbf{z}}^T \mathbf{S}_t \mathbf{M}_{\mathbf{z}} \boldsymbol{\beta}^{(j)} \quad (14)$$

and so we have

$$\int_{\mathbf{z}} J_t(h_{t|\mathbf{z}}^{(j)}) d\mathbf{z} = \boldsymbol{\beta}^{(j)T} \left[\int_{\mathbf{z}} \mathbf{M}_{\mathbf{z}}^T \mathbf{S}_t \mathbf{M}_{\mathbf{z}} d\mathbf{z} \right] \boldsymbol{\beta}^{(j)}. \quad (15)$$

This integration with respect to \mathbf{z} is still difficult to evaluate, so we apply numerical approximation techniques as in Wood (2006). Specifically, following the reparameterization method in Wood (2006), we approximate the integral in (15) by

$$\int_{\mathbf{z}} J_t(h_{t|\mathbf{z}}^{(j)}) d\mathbf{z} \approx \boldsymbol{\beta}^{(j)T} \tilde{\mathbf{S}}_t \boldsymbol{\beta}^{(j)}, \quad (16)$$

where $\tilde{\mathbf{S}}_t = \mathbf{S}'_t \otimes \mathbf{I}_q$, $\mathbf{S}'_t = \mathbf{B}^{-T} \mathbf{S}_t \mathbf{B}^{-1}$, $\mathbf{B} = (b_i(t_j^*)) \in \mathbb{R}^{m \times m}$ and $t_j^* = t_{\min} + (j-1)(t_{\max} - t_{\min})/(m-1)$, for $j = 1, \dots, m$. Here $b_i(t)$ denotes the i -th entry of $\mathbf{b}(t)$, and t_{\max} and t_{\min} denote the maximum and minimum values of the domain \mathcal{T} of t , respectively. Similarly, the penalty on $h_{\mathbf{z}|t}^{(j)}$ is computed as

$$\int_t J_{\mathbf{z}}(h_{\mathbf{z}|t}^{(j)}) dt \approx \boldsymbol{\beta}^{(j)T} \tilde{\mathbf{S}}_{\mathbf{z}} \boldsymbol{\beta}^{(j)}, \quad (17)$$

where $\tilde{\mathbf{S}}_{\mathbf{z}} = \mathbf{I}_m \otimes \mathbf{S}'_{\mathbf{z}}$, $\mathbf{S}'_{\mathbf{z}} = \mathbf{A}^{-T} \mathbf{S}_{\mathbf{z}} \mathbf{A}^{-1}$, $\mathbf{A} = (v_i(\mathbf{z}_j^*)) \in \mathbb{R}^{q \times q}$ and $\{\mathbf{z}_j^* : j = 1, \dots, q\}$ is a set of values of \mathbf{z} on a regular grid spanning the observed values of \mathbf{z} . Finally, combining (16) and (17) above, a tractable approximation to the penalty (12) for the covariance function is given by,

$$J(h) \approx \sum_{j=1}^r \lambda_t \boldsymbol{\beta}^{(j)T} \tilde{\mathbf{S}}_t \boldsymbol{\beta}^{(j)} + \sum_{j=1}^r \lambda_{\mathbf{z}} \boldsymbol{\beta}^{(j)T} \tilde{\mathbf{S}}_{\mathbf{z}} \boldsymbol{\beta}^{(j)} = \boldsymbol{\beta}^T (\lambda_t \mathbf{I}_r \otimes \tilde{\mathbf{S}}_t + \lambda_{\mathbf{z}} \mathbf{I}_r \otimes \tilde{\mathbf{S}}_{\mathbf{z}}) \boldsymbol{\beta}, \quad (18)$$

where $\boldsymbol{\beta} = \text{vec}(\boldsymbol{\Gamma})$.

We use an additional penalty, $J(\mu)$, to enforce smoothness of the mean function (3). A tractable form for this penalty is obtained by applying approximations analogous to those discussed above. In particular, we have

$$J(\mu) \approx \boldsymbol{\theta}_{\mu}^T (\lambda_t^{(\mu)} \tilde{\mathbf{S}}_t^{(\mu)} + \lambda_{\mathbf{z}}^{(\mu)} \tilde{\mathbf{S}}_{\mathbf{z}}^{(\mu)}) \boldsymbol{\theta}_{\mu} \quad (19)$$

where $\tilde{\mathbf{S}}_t^{(\mu)} = \mathbf{S}_t^{(\mu)'} \otimes \mathbf{I}_p$, $\mathbf{S}_t^{(\mu)'} = \mathbf{E}^{-T} \mathbf{S}_t^{(\mu)} \mathbf{E}^{-1}$, $\mathbf{E} = (a_i(t_j^*)) \in \mathbb{R}^{l \times l}$, and $\tilde{\mathbf{S}}_{\mathbf{z}}^{(\mu)} = \mathbf{I}_l \otimes \mathbf{S}_{\mathbf{z}}^{(\mu)'}$, $\mathbf{S}_{\mathbf{z}}^{(\mu)'} = \mathbf{F}^{-T} \mathbf{S}_{\mathbf{z}}^{(\mu)} \mathbf{F}^{-1}$, $\mathbf{F} = (c_i(\mathbf{z}_j^*)) \in \mathbb{R}^{p \times p}$. Again, $\{t_i^* : i = 1, \dots, l\}$ and $\{\mathbf{z}_i^* : i = 1, \dots, p\}$ are regularly spaced over the observed values of t and \mathbf{z} , respectively (but the number of grid points is different to before).

Combining the negative log-likelihood (10) with the roughness penalties (18) and (19), we obtain the objective function to be minimized by our supervised FPCA method, i.e.,

$$\mathcal{L} + \mathcal{P} = \sum_{n=1}^N \{\log \det \boldsymbol{\Sigma}_n + \text{tr}(\boldsymbol{\Sigma}_n \boldsymbol{\Sigma}_n^{-1})\} + \boldsymbol{\theta}_{\mu}^T (\lambda_t^{(\mu)} \tilde{\mathbf{S}}_t^{(\mu)} + \lambda_{\mathbf{z}}^{(\mu)} \tilde{\mathbf{S}}_{\mathbf{z}}^{(\mu)}) \boldsymbol{\theta}_{\mu} + \boldsymbol{\beta}^T (\lambda_t \mathbf{I}_r \otimes \tilde{\mathbf{S}}_t + \lambda_{\mathbf{z}} \mathbf{I}_r \otimes \tilde{\mathbf{S}}_{\mathbf{z}}) \boldsymbol{\beta}, \quad (20)$$

where \mathcal{L} and \mathcal{P} denote the log-likelihood and penalty terms, respectively. We use cross-validation to choose the four tuning parameters λ_t , $\lambda_{\mathbf{z}}$, $\lambda_t^{(\mu)}$, and $\lambda_{\mathbf{z}}^{(\mu)}$. The next section develops an algorithm for solving this optimization problem.

Algorithm 1 Modified gradient descent for optimizing SFPDM log-likelihood (10)

- 1: Initialize β using Algorithm 2 (below);
- 2: Initialize θ_μ to be the zero vector, and (σ_e^2) to be an appropriate small positive value;
- 3: **repeat**
- 4: Update θ_μ by gradient descent with gradient (24) and (29) until convergence;
- 5: Update β by gradient descent with gradient (26) and (30) until convergence;
- 6: Update $(\sigma_e^2)^{(k_3)}$ by gradient descent with and gradient (25) until convergence;
- 7: **until** convergence

3 Algorithm

3.1 Model Training

Given training data from a collection of latent functions, our supervised mean function and principle component functions can be obtained by optimizing (20) with coordinate descent algorithm. However, the model training is challenging because the objective function (20) is non-convex. Moreover, the computation becomes intensive when the sample size is large. For each sample, evaluating the log-likelihood and its gradients involves computing the inverse of $\Sigma_n \in \mathbb{R}^{m_n \times m_n}$, which has a computational cost of order $\mathcal{O}(m_n^3)$. Each round iteration would require a complexity of $\mathcal{O}(\sum_n m_n^3)$ by scanning through all samples.

We overcome these problems by proposing a good parameter initialization algorithm, and developing efficient ways to evaluate the objection function and its gradient. We detail the gradient descent algorithm first, and defer the discussion of parameter initialization to the end of this subsection. Our gradient descent method is described in Algorithm 1. The algorithm iteratively updates one of the parameters θ_μ , β and σ_e^2 with the other two fixed until convergence.

In our investigations, our method worked well with a number of different optimization algorithms, such as Broyden–Fletcher–Goldfarb–Shanno (BFGS) algorithm proposed by Head and Zerner (1985). However, many optimization algorithms, such as gradient descent, require selection of the step size, i.e., the tuning parameter that controls the magnitude of changes in the parameters in each iteration of the algorithm. This step size selection is computationally expensive because it requires numerous evaluations of the objective function. Fortunately, with the help of the determinant and Sherman–Morrison–Woodbury lemmas, we are able to reduce the computational cost from $\mathcal{O}(m_n^3)$ to $\mathcal{O}(r^3)$ for each sample. The following lemma presents the equivalent and more efficient expression for the log-likelihood. See the Appendix for detailed proofs.

Lemma 1. *The log-likelihood \mathcal{L} given by (10) can be equivalently expressed as*

$$\mathcal{L} \propto 2 \sum_{n=1}^N \log \det(\mathbf{F}_n) - (\sigma_e^{-2})^2 \sum_{n=1}^N \|\mathbf{h}_n\|_2^2 + \sigma_e^{-2} \sum_{n=1}^N \|\mathbf{y}_n\|_2^2. \quad (21)$$

where $\mathbf{W}_n = \mathbf{C}_n^T \mathbf{B}_n^T \mathbf{B}_n \mathbf{C}_n$, $\mathbf{g}_n = \mathbf{C}_n^T \mathbf{B}_n^T \mathbf{y}_n$, $\mathbf{h}_n = \mathbf{F}_n^{-1} \mathbf{g}_n$ and \mathbf{F}_n is the Cholesky factor of $\mathbf{I}_r + \sigma_e^{-2} \mathbf{W}_n$, i.e., $\mathbf{F}_n \mathbf{F}_n^T = \mathbf{I}_r + \sigma_e^{-2} \mathbf{W}_n$.

In order to update the parameters, we also need the gradient of the objective function with respect to the parameters. For the log-likelihood term \mathcal{L} of (20), it is straightforward to verify that the gradients with respect to $\boldsymbol{\theta}_\mu$ and σ_e^2 are

$$\frac{\partial \mathcal{L}}{\partial \boldsymbol{\theta}_\mu} = \sum_{n=1}^N 2\mathbf{H}_n^T \boldsymbol{\Sigma}_n^{-1} (\mathbf{H}_n \boldsymbol{\theta}_\mu - \mathbf{y}_n) \quad (22)$$

and

$$\frac{\partial \mathcal{L}}{\partial \sigma_e^2} = \sum_{n=1}^N \text{tr}(\boldsymbol{\Sigma}_n^{-1}) - \sum_{n=1}^N (\mathbf{y}_n - \mathbf{H}_n \boldsymbol{\theta}_\mu)^T \boldsymbol{\Sigma}_n^{-2} (\mathbf{y}_n - \mathbf{H}_n \boldsymbol{\theta}_\mu), \quad (23)$$

respectively. With a similar approach as that for the objective function in Lemma 1, we can derive equivalent efficient expressions for these gradients.

Lemma 2. *The gradient $\frac{\partial \mathcal{L}}{\partial \boldsymbol{\theta}_\mu}$ given by (22) can be expressed as*

$$\frac{\partial \mathcal{L}}{\partial \boldsymbol{\theta}_\mu} = \sum_{n=1}^N -2\sigma_e^{-2} (\mathbf{H}_n^T \mathbf{y}_n - \mathbf{H}_n^T \mathbf{H}_n \boldsymbol{\theta}_\mu) + 2\sigma_e^{-2} \mathbf{H}_n^T \mathbf{B}_n \mathbf{E}_n^T \mathbf{E}_n (\mathbf{B}_n^T \mathbf{y}_n - \mathbf{B}_n^T \mathbf{H}_n \boldsymbol{\theta}_\mu), \quad (24)$$

where $\mathbf{E}_n = \mathbf{L}_n^{-1} \mathbf{C}_n^T$ and \mathbf{L}_n is the Cholesky factor of $\sigma_e^2 \mathbf{I}_r + \mathbf{C}_n^T \mathbf{B}_n^T \mathbf{B}_n \mathbf{C}_n$, i.e., $\mathbf{L}_n \mathbf{L}_n^T = \sigma_e^2 \mathbf{I}_r + \mathbf{C}_n^T \mathbf{B}_n^T \mathbf{B}_n \mathbf{C}_n$.

Lemma 3. *The gradient $\frac{\partial \mathcal{L}}{\partial \sigma_e^2}$ given by (23) can be expressed as*

$$\frac{\partial \mathcal{L}}{\partial \sigma_e^2} = \sum_{n=1}^N [\sigma_e^{-2} m_n - \sigma_e^{-2} \text{tr}(\mathbf{E}_n^T \mathbf{E}_n \mathbf{B}_n^T \mathbf{B}_n) - \sigma_e^{-2} \mathbf{y}_n^T \mathbf{y}_n + \sigma_e^{-2} \mathbf{y}_n^T \mathbf{B}_n \mathbf{E}_n^T \mathbf{E}_n \mathbf{B}_n^T \mathbf{y}_n], \quad (25)$$

where $\mathbf{E}_n = \mathbf{L}_n^{-1} \mathbf{C}_n^T$ and \mathbf{L}_n is the Cholesky factor given in Lemma 2 above.

Next, we consider the gradient of \mathcal{L} with respect to $\boldsymbol{\beta}$. Let β_{ijk} denote the k -th element of the vector $\boldsymbol{\beta}_{ij}$. Then, the gradient of \mathcal{L} with respect to β_{ijk} can be expressed as

$$\frac{\partial \mathcal{L}}{\partial \beta_{ijk}} = \sum_{n=1}^N \left\langle \frac{\partial \mathcal{L}}{\partial \mathbf{C}_n}, \frac{\partial \mathbf{C}_n}{\partial \beta_{ijk}} \right\rangle, \quad (26)$$

where the inner product is defined as $\langle \mathbf{A}, \mathbf{B} \rangle = \text{tr}(\mathbf{A}^T \mathbf{B})$, the matrix $\frac{\partial \mathcal{L}}{\partial \mathbf{C}_n}$ is

$$\frac{\partial \mathcal{L}}{\partial \mathbf{C}_n} = 2 \times \mathbf{B}_n^T [\boldsymbol{\Sigma}_n^{-1} - \boldsymbol{\Sigma}_n^{-1} \mathbf{S}_n \boldsymbol{\Sigma}_n^{-1}] \mathbf{B}_n \mathbf{C}_n, \quad (27)$$

and $\frac{\partial \mathbf{C}_n}{\partial \beta_{ijk}}$ is the matrix with all elements 0 except that its (i, j) element is $v_k(\mathbf{z})$. Note the computation of (27) can also be simplified by next lemma.

Lemma 4. *The gradient $\frac{\partial \mathcal{L}}{\partial \mathbf{C}_n}$ given by (27) can be expressed as*

$$\frac{\partial \mathcal{L}}{\partial \mathbf{C}_n} = 2\sigma_e^{-2} (\mathbf{B}_n^T \mathbf{B}_n \mathbf{C}_n - \mathbf{B}_n^T \mathbf{K}_n \mathbf{W}_n) - 2\sigma_e^{-4} (\mathbf{B}_n^T - \mathbf{B}_n^T \mathbf{K}_n \mathbf{C}_n^T \mathbf{B}_n^T) \mathbf{S}_n (\mathbf{B}_n \mathbf{C}_n - \mathbf{K}_n \mathbf{W}_n), \quad (28)$$

where $\mathbf{W}_n = \mathbf{C}_n^T \mathbf{B}_n^T \mathbf{B}_n \mathbf{C}_n$ and $\mathbf{K}_n = \mathbf{B}_n \mathbf{C}_n \{\sigma_e^2 \mathbf{I}_r + \mathbf{W}_n\}^{-1}$.

Algorithm 2 Initial estimate of the coefficient matrix Γ

- 1: Divide the covariates domain into small bins (or regions) $\mathcal{S}_1, \dots, \mathcal{S}_U$.
- 2: Apply classical FPCA in each bin to obtain $\widehat{\Sigma}_{\mathbf{z}_u}$.
- 3: Obtain the initial estimate $\boldsymbol{\beta}^{(0)}$ by solving (31).

Besides, the gradients of the penalty term \mathcal{P} in (20) with respect to $\boldsymbol{\theta}_\mu$ and $\boldsymbol{\beta}$ are

$$\frac{\partial \mathcal{P}}{\partial \boldsymbol{\theta}_\mu} = \lambda_t^{(\mu)} (\widetilde{\mathbf{S}}_t^{(\mu)} + \widetilde{\mathbf{S}}_t^{(\mu)T}) \boldsymbol{\theta}_\mu + \lambda_{\mathbf{z}}^{(\mu)} (\widetilde{\mathbf{S}}_{\mathbf{z}}^{(\mu)} + \widetilde{\mathbf{S}}_{\mathbf{z}}^{(\mu)T}) \boldsymbol{\theta}_\mu \quad (29)$$

and

$$\frac{\partial \mathcal{P}}{\partial \boldsymbol{\beta}} = \lambda_t [(\mathbf{I}_r \otimes \widetilde{\mathbf{S}}_t) + (\mathbf{I}_r \otimes \widetilde{\mathbf{S}}_t)^T] \boldsymbol{\beta} + \lambda_{\mathbf{z}} [(\mathbf{I}_r \otimes \widetilde{\mathbf{S}}_{\mathbf{z}}) + (\mathbf{I}_r \otimes \widetilde{\mathbf{S}}_{\mathbf{z}})^T] \boldsymbol{\beta}, \quad (30)$$

respectively. Finally, the gradient of objective function is obtained by combining (26) and (30) for $\boldsymbol{\beta}$, and combining (22) and (29) for $\boldsymbol{\theta}_\mu$. These gradients are employed in Algorithm 1.

It remains to introduce a procedure to initialize $\boldsymbol{\beta}$ for Algorithm 1. This procedure relies on the classical FPCA methods which do not consider covariate information. For this purpose, we divide the covariate domain into small bins (or regions) $\mathcal{S}_1, \dots, \mathcal{S}_U$, and treat the observations in each bin having a fixed covariate \mathbf{z}_u , for $u = 1, \dots, U$. These fixed covariates \mathbf{z}_u is chosen as the mean value of covariates in each bin. Then we apply classical FPCA to the observation in each bin. This gives us an estimated covariance function $\hat{G}(t, t' | \mathbf{z}_u) = \mathbf{b}(t)^T \widehat{\Sigma}_{\mathbf{z}_u} \mathbf{b}(t')$ at fixed \mathbf{z}_u for each bin. From our model construction in (4) and (5), the model parameters can be initialized via matching $\mathbf{C}(\mathbf{z}_u; \boldsymbol{\beta})$ against the matrix square root $\widehat{\Sigma}_{\mathbf{z}_u}^{1/2}$. In particular, the parameter $\boldsymbol{\beta}$ is initialized by solving

$$\boldsymbol{\beta}^{(0)} := \arg \min_{\boldsymbol{\beta}} \sum_{u=1}^U \|\widehat{\Sigma}_{\mathbf{z}_u}^{1/2} - \mathbf{C}(\mathbf{z}_u; \boldsymbol{\beta})\|_F^2. \quad (31)$$

The loss function above is measured by the squared Frobenius norm of the difference of the matrices at each \mathbf{z}_u .

3.2 Prediction

Suppose that we have applied Algorithm 1 on the training data to learn the model parameters, and we get a new observation vector $\mathbf{y}_* = (y_*(t_1^{(*)}), \dots, y_*(t_{m_*}^{(*)}))^T$ at time points $t_1^{(*)}, \dots, t_{m_*}^{(*)}$. Coupled with this new observation is its covariate value \mathbf{z}_* . We want to fit the whole underlying latent function $x_*(t)$, and make prediction for its scores, and prediction for a new noisy observation $y_*(t)$ at any time points $t \in \mathcal{T}$.

Treating the estimated model parameters $\hat{\boldsymbol{\theta}}_\mu$, $\hat{\boldsymbol{\beta}}$ and $\hat{\sigma}_e^2$ as fixed, we first infer the scores $\boldsymbol{\xi}^{(*)}$ for the observation vector \mathbf{y}_* . In a similar way as (8) and (9), define basis matrices $\mathbf{B}_* = (\mathbf{b}(t_1^{(*)}), \dots, \mathbf{b}(t_{m_*}^{(*)}))^T$, and $\mathbf{H}_* = (\mathbf{H}(t_1^{(*)}, \mathbf{z}_*), \dots, \mathbf{H}(t_{m_*}^{(*)}, \mathbf{z}_*))^T$ for this new observation. Besides, at the covariate value \mathbf{z}_* , we compute the eigendecomposition of

$\Sigma(z_*; \hat{\beta}) = \Theta_* \mathbf{D}_* \Theta_*^T$. We can now write down the joint distribution of \mathbf{y}_* and $\xi^{(*)}$, which is multivariate Gaussian distribution whose mean vector and covariance matrix are given by

$$\begin{pmatrix} \mathbf{H}_* \hat{\theta}_\mu \\ \mathbf{0} \end{pmatrix}, \quad \text{and} \quad \begin{pmatrix} \mathbf{B}_* \Sigma(z_*; \hat{\beta}) \mathbf{B}_*^T + \hat{\sigma}_e^2 \mathbf{I} & \mathbf{B}_* \Theta_* \mathbf{D}_* \\ \mathbf{D}_* \Theta_*^T \mathbf{B}_*^T & \mathbf{D}_* \end{pmatrix}, \quad (32)$$

respectively. The score value is predicted by the conditional expectation as

$$\mathbb{E}(\xi^{(*)} | \mathbf{y}_*) = \mathbf{D}_* \Theta_*^T \mathbf{B}_*^T (\mathbf{B}_* \Sigma(z_*; \hat{\beta}) \mathbf{B}_*^T + \hat{\sigma}_e^2 \mathbf{I})^{-1} (\mathbf{y}_* - \mathbf{H}_* \hat{\theta}_\mu). \quad (33)$$

The prediction uncertainty is assessed by the conditional covariance

$$\text{Var}(\xi^{(*)} | \mathbf{y}_*) = \mathbf{D}_* - \mathbf{D}_* \Theta_*^T \mathbf{B}_*^T (\mathbf{B}_* \Sigma(z_*; \hat{\beta}) \mathbf{B}_*^T + \hat{\sigma}_e^2 \mathbf{I})^{-1} \mathbf{B}_* \Theta_* \mathbf{D}_*. \quad (34)$$

Thus, if we want to predict the value of $y_*(t)$ at time t , then the mean and variance of the predictive distribution are given by

$$\mathbf{H}(t, z_*) \hat{\theta}_\mu + \mathbf{b}(t)^T \Theta_* \mathbb{E}(\xi^{(*)} | \mathbf{y}_*), \quad (35)$$

and

$$\mathbf{b}(t)^T \Theta_* \text{Var}(\xi^{(*)} | \mathbf{y}_*) \Theta_*^T \mathbf{b}(t) + \hat{\sigma}_e^2, \quad (36)$$

respectively, see (7). If we are instead interested in the underlying latent function value $x_*(t)$, then the posterior predictive distribution will be the same except the expression for the variance will not have the $\hat{\sigma}_e^2$ term. Sometimes, such as in astronomy, measurement errors are provided with each observed value of $y_*(t)$. In this case, we modify our predictions by replacing all instances of $\hat{\sigma}_e^2$ above by the actual measurement error value (and similarly in the estimation procedure implementation).

4 Simulation Study

We now compare our SFPDM method to the supervised sparse and functional principal component (SupSFPC) method proposed by Li et al. (2016), a state-of-the-art supervised FPCA approach. SupSFPC is based on the assumption that the scores have a linear relationship with the covariates, which is often violated in practice. Furthermore, SupSFPC does not allow for irregularly spaced data and user-supplied measurement errors, whereas our approach does.

4.1 Simulation study design

We simulate a dataset of noisy realizations of $N = 7500$ latent functions. The n -th latent function $x_n(t, z)$ is a linear combination of a mean function $\mu(t, z)$ and $r = 3$ orthonormal eigenfunctions $f_j(t, z)$, $j = 1, \dots, r$. Here we set the covariate z to be univariate. We set the mean function to be $\mu(t, z) = 30(t - z)^2$, and the three eigenfunctions to be

$$f_1(t, z) = \sqrt{2} \{ \cos(\pi(t + z)) \}, \quad (37)$$

$$f_2(t, z) = \sqrt{2} \{ \sin(\pi(t + z)) \}, \quad (38)$$

$$f_3(t, z) = \sqrt{2} \{ \cos(3\pi(t - z)) \}. \quad (39)$$

To further impose dependence of the covariance structure on the covariate z we set the eigenvalues to be $\mathbf{d} = (2(z + 20), z + 10, z)$. Then scores $\boldsymbol{\xi}^{(n)}$ are sampled from a Normal distribution (see(1)) with mean $\mathbf{0}$ and covariance matrix $\mathbf{D}_z = \text{diag}(\mathbf{d})$. The number of B-spline basis functions used to capture the dependence of the mean function on t and z are set to 10 and 5, respectively, i.e., $l = 10$ and $p = 5$, see (3). The number used to capture the dependence of the eigenfunctions on t and z are set to 10 and 7, respectively, see 7. All the splines used are cubic splines and the spline $\mathbf{b}(t)$ (see Section 2.2) is orthonormalized.

Since the SupSFPC method cannot handle irregularly spaced functional data, all data generated in this section are all regular grid for easy comparison. The final dataset contains \tilde{m} noisy realizations of each function x_n , i.e.,

$$y_n(t_i, \mathbf{z}) = x_n(t_i, \mathbf{z}) + \epsilon(t_i) = \mu(t_i, \mathbf{z}) + \sum_{j=1}^r \xi_j^{(n)} f_j(t_i, \mathbf{z}) + \epsilon(t_i) = \mu(t_i, \mathbf{z}) + \mathbf{f}^T(t_i, \mathbf{z}) \boldsymbol{\xi}^{(n)} + \epsilon(t_i), \quad (40)$$

for $i = 1, \dots, \tilde{m}$, where ϵ is an independent white noise process with variance $\sigma_e^2 = 0.1$. We repeat the simulation 500 times to obtain the standard errors associated with the estimators for the mean function and eigenfunctions. We also obtain a 95% posterior interval for future observations by making use of the posterior predictive distribution variance given by (36).

4.2 Results

Because SupSFPC does not give a specific method to estimate the mean function, we only summarize the mean function estimation performance of our method in Figure 1(a). In the case of SupSFPC, we treat the average of all observed curves as the estimate of the mean function of SupSFPC. Figures 1(b), 1(c), and 1(d) compare the estimation performance of our method and SupSFPC for eigenfunction f_1 , f_2 , and f_3 , respectively. For all three eigenfunctions, our method performs better in terms of estimation accuracy. Indeed, our method recovers the true mean function and three eigenfunctions almost exactly. Error bars showing two times the standard error are plotted for both methods, but cannot be seen because the standard errors are very small.

Next, we compare the prediction accuracy of the two methods. We generate a test set each consisting of noisy observations of $N = 7500$ latent functions. Then, we fit the mean function and eigenfunctions using the training set introduced in Section 4.1. For each test set function, we estimate the scores by their conditional mean (33) computed based on a random selection of 20% of the noisy realizations generated for that function, i.e., that 20% is treated as the initially observed data. Finally, we make predictions for the remaining 80% of the observations by making use of (35). Some example predictions are shown in Figure 2. Compared with the SupSFPC method, the coverage of our approach is much closer to the nominal coverage and almost all the observations fall within their 95% posterior intervals. Table 1 gives the fraction of variation explained (FVE) for the test set for both methods, i.e.,

$$1 - \frac{\sum_{n=1}^N \sum_{i=1}^{\tilde{m}} \{y_n(t_i) - \hat{\mu}^{(n)}(t_i) - \sum_{j=1}^r \hat{\xi}_j^{(n)} \hat{f}_j^{(n)}(t_i)\}^2}{\sum_{n=1}^N \sum_{i=1}^{\tilde{m}} \{y_n(t_i) - \tilde{\mu}(t_i)\}^2}, \quad (41)$$

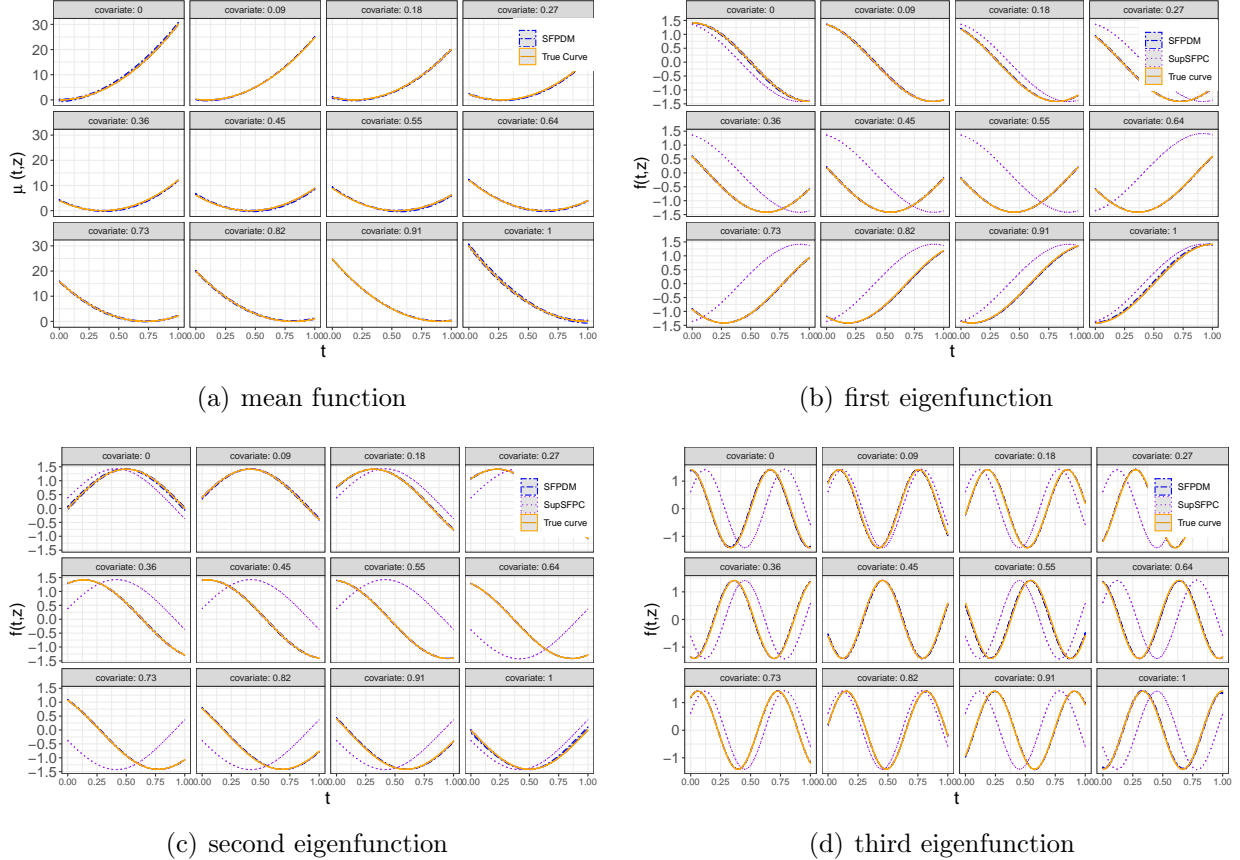


Figure 1: Panel (a) compares the SFPDM (dashed blue lines) and SupSFPC (dotted purple lines) estimates of the mean function, for a range of covariate values. Panels (b), (c), and (d) compare the SFPDM and supSFPC estimates of eigenfunctions 1, 2, and 3, respectively, for a range of covariate values. The true functions are shown as solid orange lines.

Table 1: Comparison of the test set FVE for SupSFPC and SFPDM.

r	SupSFPC	SFPDM
	FVE ($\times 10^{-1}$)	FVE($\times 10^{-1}$)
r = 1	5.9987	7.8485
r = 2	9.7460	9.8380
r = 3	9.8792	9.9837

where $\hat{\xi}$ is the estimate of the scores, and $\tilde{\mu}(t_i) = \frac{1}{N} \sum_{n=1}^N y(t_i)$, for $i = 1, \dots, \tilde{m}$. Here $\hat{\mu}$ and \hat{f} are the estimates of the mean function and eigenfunctions, which in the case of our method depend on t and z , but only depend on t for SupSFPC. Our model has a higher FVE for all three values of r .

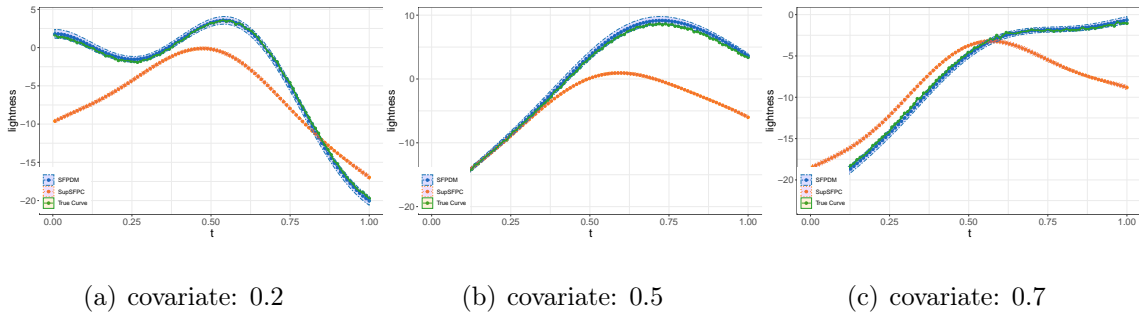


Figure 2: Panels (a), (b) and (c) show example curve predictions and 95% posterior prediction intervals for the SFPDM (blue dash-dot lines) and SupSFPC (dotted lines) methods. The green solid lines show the true curve. The covariates for the curves are given beneath the panels.

5 Modeling Astronomical Lightcurves

In astronomy, a lightcurve is a time series of the observed brightness of a source, e.g., a star or galaxy. Some astronomical sources vary in brightness over time, and these variations can be used to classify the type of source or infer its properties, e.g., the period of star pulsations (from which additional physical insights can be gained). One type of variable source is an eclipsing binary system, which is a system of two stars orbiting each other. Many stars visible to the eye are in fact eclipsing binary systems. If the orbits of the two stars lie in the plane that also contains our line of sight then, viewed from Earth, the stars will alternately eclipse each other. The stars cannot usually be resolved, but the eclipses block some of the light from reaching us and create periodic dips in the observed lightcurve. These characteristics can be used to distinguish eclipsing binary sources from other variable sources and help us to infer properties of the two stars, e.g., their relative masses.

Our data set consists of $n = 35615$ eclipsing binary lightcurves from the Catalina Real-Time Transient Survey (CRTS) (Drake et al., 2009) which were classified by the

CRTS team in Drake et al. (2014). Each observed magnitude (brightness) measurement is accompanied by a known measurement error (i.e., standard deviation), that is determined by astronomers based on the properties of the telescope used. The data are publicly available from <http://crtsn.caltech.edu/>. Figure 3(a) shows standardized versions of 10 eclipsing binary lightcurves. For visual purposes the measurement errors are not plotted; they have a median value of about 0.15 (in standardized magnitude units). The y -axis units are standardized magnitude: magnitude is an astronomical measure of the intensity of light from a star, with negative numbers indicating greater intensity. Standardizing so that all the measurements fall in $[0.5, -0.5]$ is necessary here because we are principally interested in modeling the similar shapes of the lightcurves. In Figure 3(a), we set the x -axis to be phase of oscillation, which is the conventional approach because eclipsing binary lightcurves are periodic. The period of oscillation for each lightcurve was found by Drake et al. (2014) and is treated as known for the purposes of our analysis. In practice, the periods would have to be estimated, which is itself a challenging inference problem. The improved modeling we present here will in turn facilitate improved period estimation accuracy in future.

An important feature of Figure 3(a) is that for some lightcurves the depth of the two eclipses are similar, and for others they are very different. This distinction is due to there being different types of eclipsing binary system. Eclipsing binaries are often divided into two classes, contact binaries which are sufficiently close to exchange mass, and detached binaries which are more separated. Contact binaries typically consist of two sources with similar properties (e.g., size and brightness), meaning that the two eclipses are similar. In contrast, detached binaries may have eclipses of any relative size, because the two sources can have completely different properties.

The above considerations raise an important modeling challenge: eclipsing binary lightcurves can be modeled using somewhat similar functions, because they have similar shapes and covariance structures, but it does not make sense to treat them as coming from a completely homogeneous distribution, as is typically assumed in FPCA. The current solution is to divide eclipsing binaries into contact and detached binaries and treat these groups as homogeneous, but this is still unsatisfactory because the detached binaries group is heterogeneous. Treating eclipsing binaries as homogeneous, means that any models we use to fit them will either be inaccurate or unnecessarily complicated, which in turn will reduce our ability to classify them, estimate their periods, and learn their other properties. Instead, we use our SFPDM method to learn a mean function and a set of covariance matrix eigenfunctions that smoothly vary with the relative depth of the two eclipses. This approach captures the fact that eclipsing binary lightcurves are similar, while also accounting for a physically interpretable difference.

To implement our approach we need a parameter or covariate related to the relative depth of the two eclipses of each lightcurve. In practice, such information may sometimes be available from a separate observation of the eclipsing binary system, e.g., from another telescope targeting a different light wavelength range. However, in many cases a parameter capturing the relative depth would need to be inferred from the data. For the sake of simplicity, in this work we calculate an approximation of the relative depth of the eclipses of each lightcurve from the data and treat it as a covariate.

SupSFPC only handles regularly spaced data and does make use of measurement errors.

Table 2: Comparison of prediction MSE for the grid data.

r	SupSFPC ($\times 10^{-2}$)		SFPDM($\times 10^{-2}$)	
	Training Set	Test Set	Training Set	Test Set
r = 1	1.6337	3.2535	1.9334	2.0039
r = 2	1.5335	3.2388	1.5671	1.7304
r = 3	1.4948	3.1842	0.5185	0.8649

Therefore, for the purpose of comparing our approach to SupSFPC, we first consider a processed version of the data where all the observations lie on a regular phase grid. In particular, we use a cubic spline fit to each lightcurve to obtain 101 observations at regularly spaced phases, regardless of the number of observations in the original lightcurve. For this grid data, we do not have measurement errors. After comparing the methods on the grid data, we will also apply our model to the raw data (including the measurement errors) to further demonstrate its performance.

We randomly divided the grid dataset into a training set and a test set, composed of 70% and 30% of the total number of lightcurves, respectively. Table 2 shows the training and test prediction mean square error (MSE) for both SupSFPC and our method. The predictions are computed in the same way as in Section 4.2, except a random 25% of the observations in each lightcurve are used to estimate the scores, and predictions are made for the other 75% (as opposed to 20% for estimation and 80% for prediction). The rows of Table 2 correspond to different values of r , the rank of the matrix \mathbf{C} used in approximating the covariance matrix Σ , see (5). Table 2 shows that the training set prediction MSE is similar for both methods when $r = 2$, which suggests that the effective degrees of freedom of the two models are similar in this case. However, the test set prediction MSE is much lower for our SFPDM method when $r = 2$, and in fact for all three choices of r .

Figures 3(b), 3(c), and 3(d) show 95% posterior prediction intervals for SupSFPCA (orange dotted lines) and our SFPDM method (blue dash-dot lines), for three example lightcurves in the test set. The true lightcurves are also shown (green solid lines). Our method well captures the way the lightcurve shapes vary with the covariate, and also provides reasonable posterior prediction intervals. In contrast, the SupSFPC method does not capture the lightcurve shapes well, because its assumption that the scores vary linearly with the covariate is not valid. Furthermore, the 95% posterior prediction intervals are clearly inadequate. To further demonstrate this, we define loss to be the summation of the prediction squared errors, and plot the loss for each method in Figure 4(a). SFPDM has similar loss for all values of the covariate, but SupSFPC has much higher loss for larger values of the covariate. In particular, since the SupSFPC method cannot properly capture the way the lightcurves change with the covariate, it focuses on fitting lightcurves with low covariate values, which constitute the majority of the data (and correspond to contact binaries).

Next we apply SFPDM to the raw data, which cannot be analyzed by the SupSFPC method. In this case the training and test set prediction MSE are almost identical, indicating that the model well captures the data. Figures (4(b), 4(c), and 4(d)) shows 95% posterior

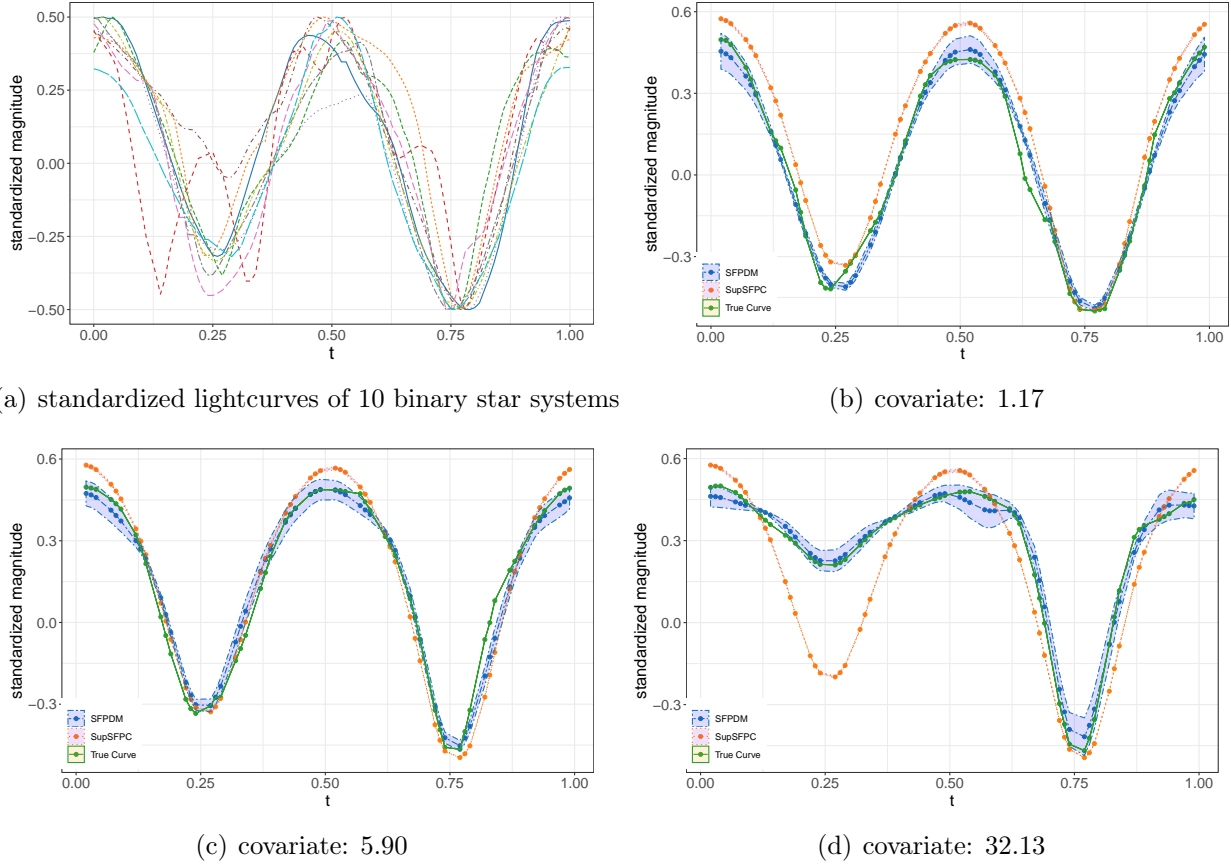


Figure 3: Panel (a) shows standardized lightcurves of 10 eclipsing binary sources. Panels (b), (c), and (d) show example lightcurve predictions and 95% posterior prediction intervals for the SFPDM (blue dash-dot lines) and SupSFPC (orange dotted lines) methods. The green solid lines show the true lightcurve. The covariates values of the three lightcurves are given beneath the panels.

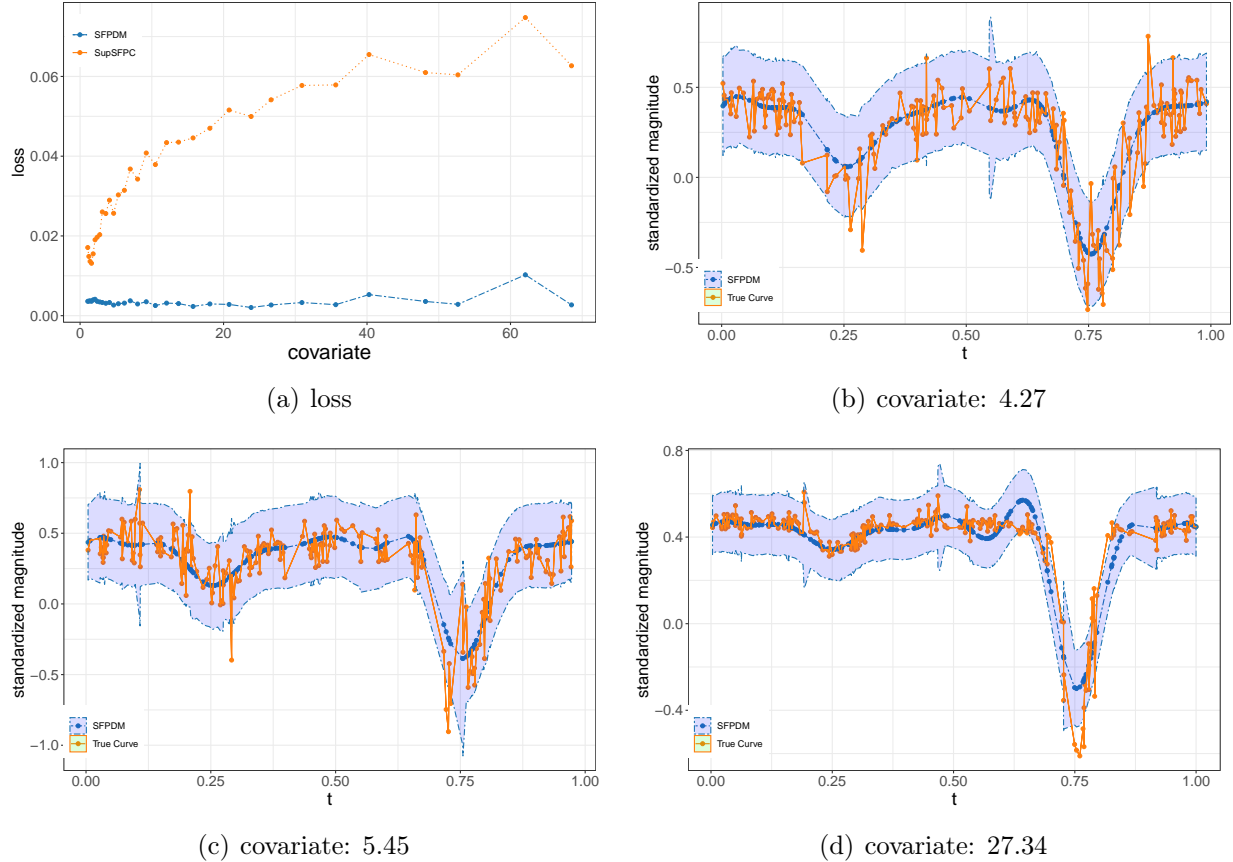


Figure 4: Panel (a) compares the loss (i.e., the prediction MSE) for SFPDM (blue dash-dot) and SupSFPC (orange dotted). Panels (b), (c) and (d) are SFPDM predictions and 95% posterior prediction intervals (blue dash-dot) for three example raw data lightcurves in the test set. The orange solid line shows the raw data. The covariate value for each lightcurve is given beneath the panels.

prediction intervals for three example lightcurves in the test set. In this the case 95% posterior prediction intervals are actually more consistent with the data than in the grid data case. This is because, for the raw data, observation-specific measurement errors are available both for fitting the model and for making predictions. Although the observation-specific measurement errors may not be available for making predictions in some special cases, we can still obtain rough estimates of the measurement error from the training data or adjacent points near the prediction.

6 Discussion

In both our simulation study and our real data analysis, our method performs better than SupSFPC in all aspects, e.g., mean and eigenfunction estimation, and prediction accuracy. Furthermore, our method can handle irregular observation times and incorporate measurement errors, whereas SupSFPC does not. By imposing a low rank structure on the matrix \mathbf{C} used in modeling the underlying covariance structure (see (5)), and applying the determinant and Sherman-Morrison-Woodbury lemmas, we reduce the the computational cost of our approach from $\mathcal{O}(m_n^3)$ to $\mathcal{O}(r^3)$. Thus, our method has substantially lower computational cost than local smoother based covariate adjustment approaches, e.g., Jiang et al. (2010), Jiang et al. (2011), Zhang et al. (2013), and Zhang et al. (2016).

To verify the above claim we compared our method with Jiang et al. (2010) in a small simulation study; it was not practical to run their method on our original simulation studies, because of its long run time. For the training data, we simulated a dataset of noisy realizations of $N = 100$ latent functions in the same way as in Section 4.1. Across 10 repetitions of the simulation, the average training time for our algorithm was 2.80 seconds compared with 15049.55 seconds for the Jiang et al. (2010) method. To compare estimation accuracy, we consider the average squared error across the observed points for each of the three eigenfunctions (the same as those in Section 4.1). The mean average squared errors for the three estimated eigenfunctions were $(0.1880, 0.2253, 0.1760)$ and $(0.2657, 0.3049, 1.8568)$ under our method and the Jiang et al. (2010) approach, respectively. In summary, our method was both more accurate and substantially more computationally efficient. The low computational cost of our method means that it is applicable to many large datasets for which local smoother based approaches are not practical.

In future work we will explore ways to construct a map from Euclidean space to the Stiefel manifold, because the coefficient matrix Θ_* (see (32)) lies on the Stiefel manifold. The Stiefel manifold has more structure than the symmetric positive semi-definite matrix manifold and optimization methods on the Stiefel manifold have been well developed, e.g., Boothby (1986), Balogh et al. (2004), Nishimori and Akaho (2005), Wen and Yin (2013).

7 Appendix

Proof of Lemma 1. We set $\mathbf{A} = \sigma_e^2 \mathbf{I}$, $\mathbf{U} = \mathbf{B}_n \mathbf{C}_n$ and $\mathbf{V} = \mathbf{B}_n \mathbf{C}_n$ so that the determinant and inverse of $\Sigma_n = \mathbf{B}_n \mathbf{C}_n \mathbf{C}_n^T \mathbf{B}_n^T + \sigma_e^2 \mathbf{I}$ are given by

$$|\Sigma_n| = \det(\mathbf{I}_r + \sigma_e^{-2} \mathbf{C}_n^T \mathbf{B}_n^T \mathbf{B}_n \mathbf{C}_n) + m_n \log \sigma_e^2 \quad (42)$$

and

$$\Sigma_n^{-1} = \sigma_e^{-2} (\mathbf{I}_{m_n} - \mathbf{B}_n \mathbf{C}_n \{\sigma_e^2 \mathbf{I}_r + \mathbf{W}_n\}^{-1} \mathbf{C}_n^T \mathbf{B}_n^T), \quad (43)$$

respectively. Similarly, using the same two lemmas, the log likelihood in (10) can be simplified to

$$\mathcal{L} \propto \sum_{n=1}^N \log \det(\mathbf{I}_r + \sigma_e^{-2} \mathbf{W}_n) + \text{tr}(\sigma_e^{-2} \mathbf{S}_n [\mathbf{I}_{m_n} - \mathbf{B}_n \mathbf{C}_n \{\sigma_e^2 \mathbf{I}_r + \mathbf{W}_n\}^{-1} \mathbf{C}_n^T \mathbf{B}_n^T]), \quad (44)$$

where $\mathbf{W}_n = \mathbf{C}_n^T \mathbf{B}_n^T \mathbf{B}_n \mathbf{C}_n$.

The steps to obtain this simplification are as follows:

$$\begin{aligned} \mathcal{L} &= \sum_{n=1}^N \log \det(\mathbf{I}_r + \sigma_e^{-2} \mathbf{C}_n^T \mathbf{B}_n^T \mathbf{B}_n \mathbf{C}_n) + m_n \log \sigma_e^2 \\ &\quad + \text{tr}(\sigma_e^{-2} \mathbf{S}_n [\mathbf{I}_{m_n} - \mathbf{B}_n \mathbf{C}_n \{\sigma_e^2 \mathbf{I}_r + \mathbf{C}_n^T \mathbf{B}_n^T \mathbf{B}_n \mathbf{C}_n\}^{-1} \mathbf{C}_n^T \mathbf{B}_n^T]) \end{aligned} \quad (45)$$

$$\begin{aligned} &\propto \sum_{n=1}^N \log \det(\mathbf{I}_r + \sigma_e^{-2} \mathbf{C}_n^T \mathbf{B}_n^T \mathbf{B}_n \mathbf{C}_n) \\ &\quad + \text{tr}(\sigma_e^{-2} \mathbf{S}_n [\mathbf{I}_{m_n} - \mathbf{B}_n \mathbf{C}_n \{\sigma_e^2 \mathbf{I}_r + \mathbf{C}_n^T \mathbf{B}_n^T \mathbf{B}_n \mathbf{C}_n\}^{-1} \mathbf{C}_n^T \mathbf{B}_n^T]) \end{aligned} \quad (46)$$

$$\propto \sum_{n=1}^N \log \det(\mathbf{I}_r + \sigma_e^{-2} \mathbf{W}_n) + \text{tr}(\sigma_e^{-2} \mathbf{S}_n [\mathbf{I}_{m_n} - \mathbf{B}_n \mathbf{C}_n \{\sigma_e^2 \mathbf{I}_r + \mathbf{W}_n\}^{-1} \mathbf{C}_n^T \mathbf{B}_n^T]),$$

where $\mathbf{W}_n = \mathbf{C}_n^T \mathbf{B}_n^T \mathbf{B}_n \mathbf{C}_n$.

To further reduce computational cost, we use a Cholesky decomposition when evaluating the log-likelihood. Firstly, note that

$$\mathcal{L} \propto \sum_{n=1}^N \log \det(\mathbf{I}_r + \sigma_e^{-2} \mathbf{W}_n) + \text{tr}(\sigma_e^{-2} \mathbf{S}_n) - \text{tr}(\sigma_e^{-2} \mathbf{S}_n \mathbf{B}_n \mathbf{C}_n \{\sigma_e^2 \mathbf{I}_r + \mathbf{W}_n\}^{-1} \mathbf{C}_n^T \mathbf{B}_n^T) \quad (47)$$

$$\propto \sum_{n=1}^N [\log \det(\mathbf{I}_r + \sigma_e^{-2} \mathbf{W}_n) - (\sigma_e^{-2})^2 \text{tr}(\mathbf{g}_n^T \{\mathbf{I}_r + \sigma_e^{-2} \mathbf{W}_n\}^{-1} \mathbf{g}_n)] + \sigma_e^{-2} \sum_{n=1}^N \|\mathbf{y}_n\|_2^2, \quad (48)$$

where $\mathbf{g}_n = \mathbf{C}_n^T \mathbf{B}_n^T \mathbf{y}_n$. Thus, if we compute the Cholesky factor of $\mathbf{I}_r + \sigma_e^{-2} \mathbf{W}_n$, that is $\mathbf{I}_r + \sigma_e^{-2} \mathbf{W}_n = \mathbf{F}_n \mathbf{F}_n^T$, and set $\mathbf{h}_n = \mathbf{F}_n^{-1} \mathbf{g}_n$, then the objective function can be expressed as

$$\mathcal{L} \propto 2 \sum_{n=1}^N \log \det(\mathbf{F}_n) - (\sigma_e^{-2})^2 \sum_{n=1}^N \|\mathbf{h}_n\|_2^2 + \sigma_e^{-2} \sum_{n=1}^N \|\mathbf{y}_n\|_2^2. \quad (49)$$

□

Proof of Lemma 2. We use a similar approach as in the proof of Lemma 1 to reduce the computational cost of evaluating the log-likelihood gradients. The gradient of the log-likelihood with respect to $\boldsymbol{\theta}_\mu$ (given in (22)) can be simplified to

$$\frac{\partial \mathcal{L}}{\partial \boldsymbol{\theta}_\mu} = \sum_{n=1}^N -2\sigma_e^{-2}(\mathbf{H}_n^T \mathbf{y}_n - \mathbf{H}_n^T \mathbf{H}_n \boldsymbol{\theta}_\mu) + 2\sigma_e^{-2} \mathbf{H}_n^T \mathbf{B}_n \mathbf{E}_n^T \mathbf{E}_n (\mathbf{B}_n^T \mathbf{y}_n - \mathbf{B}_n^T \mathbf{H}_n \boldsymbol{\theta}_\mu), \quad (50)$$

where $\mathbf{E}_n = \mathbf{L}_n^{-1} \mathbf{C}_n^T$ and \mathbf{L}_n is the Cholesky factor of $\sigma_e^2 \mathbf{I}_r + \mathbf{C}_n^T \mathbf{B}_n^T \mathbf{B}_n \mathbf{C}_n$, i.e. $\mathbf{L}_n \mathbf{L}_n^T = \sigma_e^2 \mathbf{I}_r + \mathbf{C}_n^T \mathbf{B}_n^T \mathbf{B}_n \mathbf{C}_n$. \square

This result is obtained by applying Sherman-Morrison-Woodbury lemma, (see (43)). The steps to obtain this simplification are as follows:

$$\frac{\partial \mathcal{L}}{\partial \boldsymbol{\theta}_\mu} = \sum_{n=1}^N 2\sigma_e^{-2} \mathbf{H}_n^T [\mathbf{I}_{m_n} - \mathbf{B}_n \mathbf{C}_n (\sigma_e^2 \mathbf{I}_r + \mathbf{C}_n^T \mathbf{B}_n^T \mathbf{B}_n \mathbf{C}_n)^{-1} \mathbf{C}_n^T \mathbf{B}_n^T] (\mathbf{H}_n \boldsymbol{\theta}_\mu - \mathbf{y}_n) \quad (51)$$

$$= \sum_{n=1}^N 2\sigma_e^{-2} \mathbf{H}_n^T [\mathbf{I}_{m_n} - \mathbf{B}_n \mathbf{C}_n (\mathbf{L}_n \mathbf{L}_n^T)^{-1} \mathbf{C}_n^T \mathbf{B}_n^T] (\mathbf{H}_n \boldsymbol{\theta}_\mu - \mathbf{y}_n) \quad (52)$$

$$= \sum_{n=1}^N -2\sigma_e^{-2} (\mathbf{H}_n^T \mathbf{y}_n - \mathbf{H}_n^T \mathbf{H}_n \boldsymbol{\theta}_\mu) + 2\sigma_e^{-2} \mathbf{H}_n^T \mathbf{B}_n \mathbf{E}_n^T \mathbf{E}_n (\mathbf{B}_n^T \mathbf{y}_n - \mathbf{B}_n^T \mathbf{H}_n \boldsymbol{\theta}_\mu), \quad (53)$$

Proof of Lemma 3. Similarly to the proof of Lemma 2, the gradient of the log likelihood with respect to σ_e^2 (given in (23)) can be simplified to

$$\frac{\partial \mathcal{L}}{\partial \sigma_e^2} = \sum_{n=1}^N \text{tr}(\boldsymbol{\Sigma}_n^{-1}) - (\boldsymbol{\Sigma}_n^{-1} \mathbf{y}_n)^T (\boldsymbol{\Sigma}_n^{-1} \mathbf{y}_n) \quad (54)$$

$$= \sum_{n=1}^N [\sigma_e^{-2} m_n - \sigma_e^{-2} \text{tr}(\mathbf{E}_n^T \mathbf{E}_n \mathbf{B}_n^T \mathbf{B}_n) - (\boldsymbol{\Sigma}_n^{-1} \mathbf{y}_n)^T (\boldsymbol{\Sigma}_n^{-1} \mathbf{y}_n)], \quad (55)$$

where $\boldsymbol{\Sigma}_n^{-1} \mathbf{y}_n = \sigma_e^{-2} \mathbf{y}_n - \sigma_e^{-2} \mathbf{B}_n \mathbf{E}_n^T \mathbf{E}_n \mathbf{B}_n^T \mathbf{y}_n$ and \mathbf{E}_n is defined in lemma 2. The steps to obtain the simplification of $\text{tr}(\boldsymbol{\Sigma}_n^{-1})$ in (55) are as follows:

$$\text{tr}(\boldsymbol{\Sigma}_n^{-1}) = \sigma_e^{-2} \text{tr} [\mathbf{I}_{m_n} - \mathbf{B}_n \mathbf{C}_n (\sigma_e^2 \mathbf{I}_r + \mathbf{C}_n^T \mathbf{B}_n^T \mathbf{B}_n \mathbf{C}_n)^{-1} \mathbf{C}_n^T \mathbf{B}_n^T] \quad (56)$$

$$= \sigma_e^{-2} m_n - \sigma_e^{-2} \text{tr}(\mathbf{E}_n^T \mathbf{E}_n \mathbf{B}_n^T \mathbf{B}_n), \quad (57)$$

\square

Proof of Lemma 4. Using Sherman-Morrison-Woodbury lemmas, we replace $\boldsymbol{\Sigma}_n^{-1}$ in (27) by

$$\sigma_e^{-2} (\mathbf{I}_{m_n} - \mathbf{B}_n \mathbf{C}_n \{\sigma_e^2 \mathbf{I}_r + \mathbf{W}_n\}^{-1} \mathbf{C}_n^T \mathbf{B}_n^T), \quad (58)$$

where $\mathbf{W}_n = \mathbf{C}_n^T \mathbf{B}_n^T \mathbf{B}_n \mathbf{C}_n$. Then, the final form of $\frac{\partial \mathcal{L}}{\partial \mathbf{C}_n}$ is

$$\frac{\partial \mathcal{L}}{\partial \mathbf{C}_n} = 2\sigma_e^{-2} (\mathbf{B}_n^T \mathbf{B}_n \mathbf{C}_n - \mathbf{B}_n^T \mathbf{K}_n \mathbf{W}_n) - 2(\sigma_e^2)^{-2} (\mathbf{B}_n^T - \mathbf{B}_n^T \mathbf{K}_n \mathbf{C}_n^T \mathbf{B}_n^T) \mathbf{S}_n (\mathbf{B}_n \mathbf{C}_n - \mathbf{K}_n \mathbf{W}_n),$$

where $\mathbf{K}_n = \mathbf{B}_n \mathbf{C}_n \{\sigma_e^2 \mathbf{I}_r + \mathbf{W}_n\}^{-1}$. \square

References

Balogh, J., Csendes, T., and Rapcsák, T. (2004), “Some global optimization problems on Stiefel manifolds,” *Journal of Global Optimization*, 30, 91–101.

Boothby, W. M. (1986), *An introduction to differentiable manifolds and Riemannian geometry*, vol. 120, Academic press.

Butterfield, K. R. (1976), “The computation of all the derivatives of a B-spline basis,” *IMA Journal of Applied Mathematics*, 17, 15–25.

Cai, T., and Yuan, M. (2010), “Nonparametric covariance function estimation for functional and longitudinal data,” *University of Pennsylvania and Georgia inistitute of technology*.

De Boor, C. (1977), “Package for calculating with B-splines,” *SIAM Journal on Numerical Analysis*, 14, 441–472.

Di, C.-Z., Crainiceanu, C. M., Caffo, B. S., and Punjabi, N. M. (2009), “Multilevel functional principal component analysis,” *The annals of applied statistics*, 3, 458.

Drake, A., Djorgovski, S., Mahabal, A., Beshore, E., Larson, S., Graham, M., Williams, R., Christensen, E., Catelan, M., Boattini, A. et al. (2009), “First results from the catalina real-time transient survey,” *The Astrophysical Journal*, 696, 870.

Drake, A., Graham, M., Djorgovski, S., Catelan, M., Mahabal, A., Torrealba, G., García-Álvarez, D., Donalek, C., Prieto, J., Williams, R. et al. (2014), “The catalina surveys periodic variable star catalog,” *The Astrophysical Journal Supplement Series*, 213, 9.

Head, J. D., and Zerner, M. C. (1985), “A Broyden—Fletcher—Goldfarb—Shanno optimization procedure for molecular geometries,” *Chemical physics letters*, 122, 264–270.

James, G. M., Hastie, T. J., and Sugar, C. A. (2000), “Principal component models for sparse functional data,” *Biometrika*, 87, 587–602.

Jiang, C.-R., Wang, J.-L. et al. (2010), “Covariate adjusted functional principal components analysis for longitudinal data,” *The Annals of Statistics*, 38, 1194–1226.

— (2011), “Functional single index models for longitudinal data,” *The Annals of Statistics*, 39, 362–388.

Kayano, M., and Konishi, S. (2009), “Functional principal component analysis via regularized Gaussian basis expansions and its application to unbalanced data,” *Journal of Statistical Planning and Inference*, 139, 2388–2398.

Li, G., Shen, H., and Huang, J. Z. (2016), “Supervised sparse and functional principal component analysis,” *Journal of Computational and Graphical Statistics*, 25, 859–878.

Lin, L., St. Thomas, B., Zhu, H., and Dunson, D. B. (2017), “Extrinsic local regression on manifold-valued data,” *Journal of the American Statistical Association*, 112, 1261–1273.

Nishimori, Y., and Akaho, S. (2005), “Learning algorithms utilizing quasi-geodesic flows on the Stiefel manifold,” *Neurocomputing*, 67, 106–135.

Paul, D., Peng, J. et al. (2009), “Consistency of restricted maximum likelihood estimators of principal components,” *The Annals of Statistics*, 37, 1229–1271.

Peng, J., and Paul, D. (2009), “A geometric approach to maximum likelihood estimation of the functional principal components from sparse longitudinal data,” *Journal of Computational and Graphical Statistics*, 18, 995–1015.

Ramsay, J., and Silverman, B. (2005), “Principal components analysis for functional data,” *Functional Data Analysis*, 147–172.

Suarez, A. J., Ghosal, S. et al. (2017), “Bayesian estimation of principal components for functional data,” *Bayesian Analysis*, 12, 311–333.

Van Der Linde, A. (2008), “Variational bayesian functional PCA,” *Computational Statistics & Data Analysis*, 53, 517–533.

Wen, Z., and Yin, W. (2013), “A feasible method for optimization with orthogonality constraints,” *Mathematical Programming*, 142, 397–434.

Wood, S. N. (2006), “Low-rank scale-invariant tensor product smooths for generalized additive mixed models,” *Biometrics*, 62, 1025–1036.

Yao, F., Müller, H.-G., and Wang, J.-L. (2005), “Functional data analysis for sparse longitudinal data,” *Journal of the American Statistical Association*, 100, 577–590.

Zhang, X., Park, B. U., and Wang, J.-l. (2013), “Time-varying additive models for longitudinal data,” *Journal of the American Statistical Association*, 108, 983–998.

Zhang, X., Wang, J.-L. et al. (2016), “From sparse to dense functional data and beyond,” *The Annals of Statistics*, 44, 2281–2321.

Zhou, L., Huang, J. Z., and Carroll, R. J. (2008), “Joint modelling of paired sparse functional data using principal components,” *Biometrika*, 95, 601–619.

Zhu, H., Chen, Y., Ibrahim, J. G., Li, Y., Hall, C., and Lin, W. (2009), “Intrinsic Regression Models for Positive-Definite Matrices With Applications to Diffusion Tensor Imaging,” *Journal of the American Statistical Association*, 104, 1203–1212, pMID: 20174601.